metals

MDPI

Article

Numerical Study on Heat Transfer Characteristic of Hot Metal Transportation before EAF Steelmaking Process

Weizhen Chen, Hang Hu, Shuai Wang, Feng Chen, Yufeng Guo and Lingzhi Yang *

School of Minerals Processing and Bioengineering, Central South University, Changsha 410083, China; csu-chenweizhen@csu.edu.cn (W.C.); csu-huhang@csu.edu.cn (H.H.); wang_shuai@csu.edu.cn (S.W.); csuchenf@csu.edu.cn (F.C.); yfguo@csu.edu.cn (Y.G.)
* Correspondence: yanglingzhi@csu.edu.cn

Abstract: The temperature of hot metal (HM) is crucial for the energy input and smelting in the electric arc furnace (EAF) steelmaking process with HM and scrap as the charge structure. However, due to the influence of many factors in the heat dissipation in HM transportation before the EAF steelmaking process, the temperature drop of HM before charged is usually fluctuating and uncertain. This situation is not conducive to the input energy control and energy optimization of the EAF steelmaking process. In this paper, a three-dimensional numerical model of a 90-ton hot metal ladle is established to simulate the heat transfer characteristic of HM transportation through ANSYS Fluent 2023 and verified by on-the-spot testing and sample analysis. The effects of ambient temperature, air velocity, slag thickness and furnace cover thickness on the temperature drop of HM are investigated and quantitatively analyzed in 30 numerical schemes. The results indicate that slag thickness is the most influential factor, followed by furnace cover thickness, air velocity and ambient temperature. In the case of 50 min transport time, the temperature drop of HM is 55.2, 15.06, 12.08, 10.38, 10.29 and 10.26 °C when the slag thickness is 0, 50, 100, 150, 200 and 250 mm, respectively. While HM is not covered by slag, the furnace cover can also greatly reduce the temperature drop. Based on the simulated data, a prediction model of HM temperature drop is obtained through the multi-factor coupling analysis and mathematical fitting. This study can help develop targeted insulation measures and determine the temperature of HM, which is expected to control the input energy for deep energy-saving optimization in the EAF steelmaking process.

Keywords: numerical simulation; heat transfer characteristic; temperature drop; hot metal transportation; slag thickness

check for updates

Citation: Chen, W.; Hu, H.; Wang, S.; Chen, F.; Guo, Y.; Yang, L. Numerical Study on Heat Transfer Characteristic of Hot Metal Transportation before EAF Steelmaking Process. *Metals* **2024**, *14*, 673. https://doi.org/10.3390/met14060673

Academic Editor: Corby G. Anderson

Received: 24 April 2024
Revised: 30 May 2024
Accepted: 3 June 2024
Published: 6 June 2024

Copyright: © 2024 by the authors. Licensee MDPI, Basel, Switzerland. This article is an open access article distributed under the terms and conditions of the Creative Commons Attribution (CC BY) license (https://creativecommons.org/licenses/by/4.0/).

1. Introduction

The electric arc furnace (EAF) steelmaking process can reduce CO_2 emissions by 63~73% compared with blast furnace and basic oxygen furnace [1,2]. The EAF steelmaking process has the advantages of a diversified charge structure, low investment, low cost and environmental safety [3,4]. In the modern EAF steelmaking process in China, the increase in the ratio between the quality of hot metal (HM) and the quality of scrap can reduce the out-of-spec steel products and the consumption of electric energy, which has better economic benefits [5]. However, with the development of the energy model and automation of EAF steelmaking, it is necessary to determine the energy and temperature of HM before charged into EAF using HM and scrap [6]. Limited by the influence of many factors on the heat dissipation in HM transportation, the temperature drop of HM is usually fluctuating and uncertain. Therefore, reducing the energy loss in HM transportation and establishing the mathematical model of HM temperature drop are of great significance for energy saving, emission reduction and production cost reduction in the EAF steelmaking process.

A large number of researchers have studied the heat transfer characteristic of HM transportation and made remarkable progress in the mathematical modeling of HM temperature drop and heat insulation of HM. Omotani et al. [7] studied the thermal state of

a hot metal ladle (HML) composed of different refractory materials through theoretical calculation. It was found that a 90 t ladle lined with high aluminum bricks dissipated more heat than a ladle lined with clay bricks. Zeng et al. [8] used the heat transfer theory to analyze the influencing factors of temperature drop during HM transportation. It could be found that most of the heat is lost by the HM surface. Pan et al. [9] used the numerical method of computational fluid dynamics to simulate the fluid flow and heat transfer in the ladle. The thermal stratification was caused by natural convection during the heat preservation process of the ladle before pouring, and the simulation results were verified in a water model. Du et al. [10] established a mathematical model of HM temperature drop according to the heat dissipation phenomenon during HM transportation. The results showed that the temperature drop rate in each process was different, and the temperature drop rate in the iron receiving process was the largest of all processes compared with the iron loading process, pretreatment process and transportation. By combining theoretical analysis with experimental data, Zimmer et al. [11] investigated the heat transfer behavior in a steelmaking ladle. The temperature distribution of the ladle was affected by thermal contact resistance. Furthermore, the heat dissipation of the ladle also depended on the previous process. Tripathi et al. [12] used the fluid dynamics calculation (CFD) method to establish a temperature prediction model of molten steel in the steelmaking ladle based on a mathematical model. The results showed that increasing the initial temperature of the refractory can significantly reduce the temperature drop of molten steel. However, the effect of ladle life on the temperature drop of molten steel was insignificant. Putan et al. [13,14] found that the bottom molten steel temperature drop rate was the fastest. The temperature difference between the top and bottom of molten steel reached 12 K. Adjusting the slag thickness is one of the important means to reduce the temperature drop of molten steel. Deodhar et al. [15] analyzed the temperature distribution of molten steel at slag thicknesses of 60 mm and 120 mm. It was found that with the increase in static time and slag thickness, the thermal stratification is more obvious. Yang et al. [16] studied the influencing factors in HM heat loss and pointed out that the work of reducing the temperature drop of HM should start from the aspects of process layout, HM transportation mode and heat preservation measures. Jose et al. [17] proposed a temperature prediction model of HM on a BF–BOF interface using multivariate adaptive regression splines techniques. This model significantly improved previous temperature prediction errors, whose mean absolute error of predictions was 11.2 K. A fluid–solid heat transfer 3D model for online preheating HML was established by Zhang et al. [18]. The average temperature of the working lining of the ladle could be raised by about 72.5–130.3 K using 10–30 min of online preheating during the empty ladle process. These researchers took into account a number of factors that affect the temperature drop of HM, including the amount of iron, refractories and process operations. However, the effects of air velocity, ambient temperature, slag thickness and furnace cover thickness on the temperature drop of HM were not studied. These effects are critical for the prediction models of HM temperature drop.

In this study, a 90 t HML from a plant was selected as the research subject. A three-dimensional (3D) transient simulation was conducted using Fluent 2023 R1 software, considering the boundary conditions, operating conditions and model parameters of HML. Taking into account the fluidity of HM, the study examined the effects of air velocity, ambient temperature, slag thickness and furnace cover thickness on the heat transfer behavior of HML during transportation. Experimental validation was conducted. The primary focus of this paper was to calculate the temperature drop of HM by simulating the actual heat transfer behavior of HML and develop the prediction models for HM temperature drop under tested conditions.

2. Numerical Simulation

2.1. Process Description

The steel production process and iron-containing charge allocation at Hengyang Steel Company (Hengyang, China) are shown in Figure 1, which mainly includes the HM produc-

tion process, the HM distribution process of the tank station, the HM distribution process with HML and the EAF steelmaking process. The HM from the blast furnace is transported to the tank station. The function of the tank station is to measure the temperature and weight of HM in large HML. Simultaneously, based on the subsequent line's iron composition requirements and the necessary quantity of iron in the EAF steelmaking process, the HM from the large ladle is allocated to the corresponding small HMLs. The small HMLs then transport the HM to the respective EAFs. However, the temperature measurement of HM is not set up before entering the EAF, resulting in an unknown temperature of HM. The fluctuation in the average temperature of the HM into the EAF would affect the determination of the high temperature physical heat. Hence, there is an urgent need to obtain the accurate average temperature and energy of the HM before charging in the EAF.

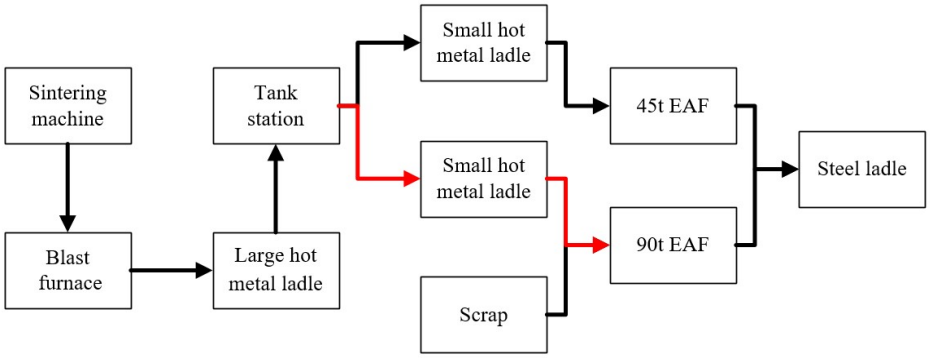


Figure 1. Steel production process and iron-containing charge allocation in the steel plant.

The temperature of HM is generally measured using thermocouples. The thermocouples can only measure the temperature of one spot. It is difficult to determine the average temperature of HM. Temperature measurement with thermocouples has the disadvantages of danger, high cost and long temperature measurement time. Numerical simulation can provide all information on the temperature and heat loss of both the HM and the HML at any particular time. Moreover, due to the absence of a temperature measurement process, the predictive model for the temperature drop of HM obtained through numerical simulation reduces the heat loss of HM. Therefore, an alternative numerical simulation method is applied to solve the problem.

2.2. Calculation Assumptions

To reduce computational complexity, improve computational efficiency and reflect the objective temperature field distribution, it is necessary to simplify and assume the heat transfer process and the geometric parameters of HML. Some specific simplifications and assumptions are as follows:

(1) The auxiliary structure on the outside of the HML is ignored. And the three-dimensional geometric model is used for calculation.

(2) The contact thermal resistance between the materials of each layer of the HM clad structure and between the refractory material and the clad steel shell is neglected. The physical properties of various materials are all homogeneous, and the erosion phenomenon and chemical reaction between the HM, refractory material, slag and air are not considered.

(3) Regardless of the flow of the slag, the friction between the slag and HM is neglected. The heat transfer of the slag is convective heat transfer and radiation heat transfer to the outside.

(4) The furnace cover has good contact with other materials, and any air leakage is negligible. When considering weather conditions, it is assumed that it is overcast with no direct sunlight and no rainfall.

Due to the above assumptions and the application of simplification measures, the simulation results of this study should be regarded as a rough indication of the thermal

behavior of HM in a ladle. These assumptions simplify the model calculation but also limit the accuracy of the simulation results. For example, ignoring contact thermal resistance may lead to overestimation of heat transfer efficiency, and ignoring slag flow makes dynamic thermal behavior impossible to accurately reflect. Therefore, further experimental research and practical application verification are still necessary.

2.3. Governing Equation

A 3D numerical model of heat transfer in HML was established. The flow and heat transfer process of HM were described in detail. The basic governing equations are summarized as follows:

(1) The continuity equation of the flowing HM is as follows [19]:

$$\frac{\partial \rho}{\partial t} + \nabla \cdot \rho u = 0 \tag{1}$$

where ρ is density of HM, kg/m^3; t is the flow time, s; u is the velocity vector, m/s.

(2) The momentum conservation equation of the flowing HM is as follows [20]:

$$\rho \frac{\partial u}{\partial t} + u \cdot \nabla (\rho u) = -\nabla P + \mu_{eff} \nabla^2 u \tag{2}$$

where P is the pressure on the fluid microbody, Pa; μ_{eff} is the effective turbulent viscosity, kg/(m·s).

(3) The turbulence equation of the flowing HM is as follows:

The standard $k - \varepsilon$ model is applied to solve the turbulent kinetic energy k and turbulent diffusivity ε in the turbulence model. The effective turbulent viscosity is obtained.

$$\mu_{eff} = \mu + \mu_t = \rho C_\mu \frac{k^2}{\varepsilon} \tag{3}$$

where μ is the molecular viscosity, kg/(m·s); μ_t is the turbulent viscosity, kg/(m·s); C_μ is a constant, which is set as 0.09 [21].

The turbulent flow energy equation is as follows:

$$\rho \frac{\partial k}{\partial t} + \rho \frac{\partial k \mu_i}{\partial x_i} = \frac{\partial}{\partial x_i} \left[\left(\mu + \frac{\mu_t}{\sigma_k} \right) \frac{\partial k}{\partial x_j} \right] + G_k - \rho \varepsilon \tag{4}$$

$$G_k = \mu_t \frac{\partial u_j}{\partial x_i} \left(\frac{\partial u_i}{\partial x_j} + \frac{\partial u_j}{\partial x_i} \right) \tag{5}$$

where u_i and u_j are the velocity component in Cartesian coordinates; x_i and x_j are the displacement component in Cartesian coordinates; G_k is the turbulent flow energy due to the velocity gradient; σ_k is a constant set as 0.09.

The turbulent diffusivity equation is as follows:

$$\rho \frac{\partial \varepsilon}{\partial t} + \rho \frac{\partial \varepsilon u_i}{\partial x_i} = \frac{\partial}{\partial x_j} \left[\left(\mu + \frac{\mu_t}{\sigma_\varepsilon} \right) \frac{\partial \varepsilon}{\partial x_j} \right] + G_{1\varepsilon} \frac{\varepsilon}{k} G_k - G_{2\varepsilon} \rho \frac{\varepsilon^2}{k} \tag{6}$$

where σ_ε, $G_{1\varepsilon}$ and $G_{2\varepsilon}$ are constants, which are set as 1.30, 1.38 and 1.92, respectively [22].

(4) The energy equation in the fluid domain is as follows:

$$\frac{\partial (\rho_1 H_1)}{\partial t} + \nabla \cdot \vec{v} (\rho_1 H_1) = \nabla \cdot \left(k_{eff} \Delta T \right) \tag{7}$$

$$k_{eff} = k_f + k_t \tag{8}$$

where H_1 is the enthalpy of the fluid, J/kg; k_{eff} is the effective thermal conductivity of the fluid, W/(m·K); k_t is the thermal conductivity of the fluid, W/(m·K); k_f is the thermal conductivity of turbulent flow, W/(m·K).

The energy equation in the solid domain is as follows:

$$\frac{\partial(\rho_s H_s)}{\partial t} = \nabla \cdot (k_s \Delta T) \tag{9}$$

where ρ_s is the density of the solid, kg/m^3; H_s is solid enthalpy, J/kg; k_s is the thermal conductivity of solid materials, W/(m·K).

(5) The Boussinesq model of the flowing HM is as follows [23]:

$$(\rho - \rho_0)g = -\rho_0 \beta (T_{st} - T_0)g \tag{10}$$

where ρ_0 is the initial density, kg/m^3; g is the acceleration of gravity set as 9.8 m/s^2; β is the thermal expansion coefficient of HM set as 2×10^{-4} K^{-1}; T_{st} is the HM temperature, K; T_0 is the reference temperature, K.

2.4. Geometric Model and Grid Model

The actual capacity of the HML is 70 t. The height of the molten iron is calculated as 1330 mm. Based on the physical dimensions of the HML, its geometric models were generated in the SPACECLAIM 2023 R1 software. The geometric models applied in the numerical simulation are shown in Figure 2. The HML is composed of steel shell and firebrick. HM is added as a fluid. The HM is covered with a layer of slag. The slag is a fluid. Due to the high viscosity of the slag, it is almost stationary. The slag is set to the solid domain to simplify the calculation. When there is no furnace cover, both the outside of the HML and the slag are subjected to comprehensive heat transfer by convection radiation. Hence, there is no specific air zone. When there is a furnace cover, there is a specific air zone between the furnace cover and the HM. HM dissipates heat directly with the specific air zone. Incorporating the furnace cover into the geometric model of the HML makes it more complex.

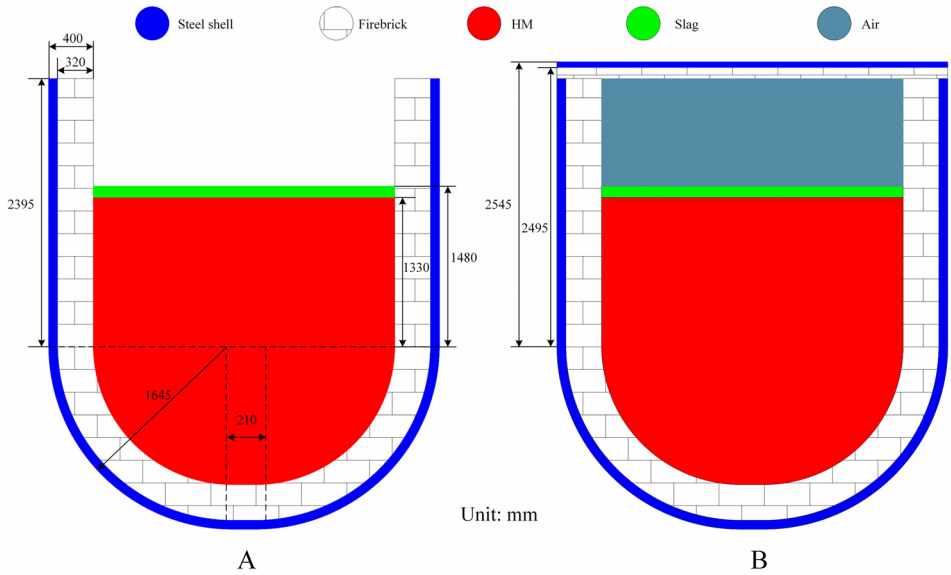


Figure 2. HML without furnace cover (**A**) and HML with a furnace cover (**B**).

In this paper, ICEM CFD 2023 R1 is used to complete the meshing work and convert the structured mesh into an unstructured mesh. The mesh model of the HML is shown in Figure 3. Since the temperature gradient of the area near the wall is relatively large, the boundary layer grid is set at this area. This can reduce the error of the simulation calculation and improve the convergence of the calculation.

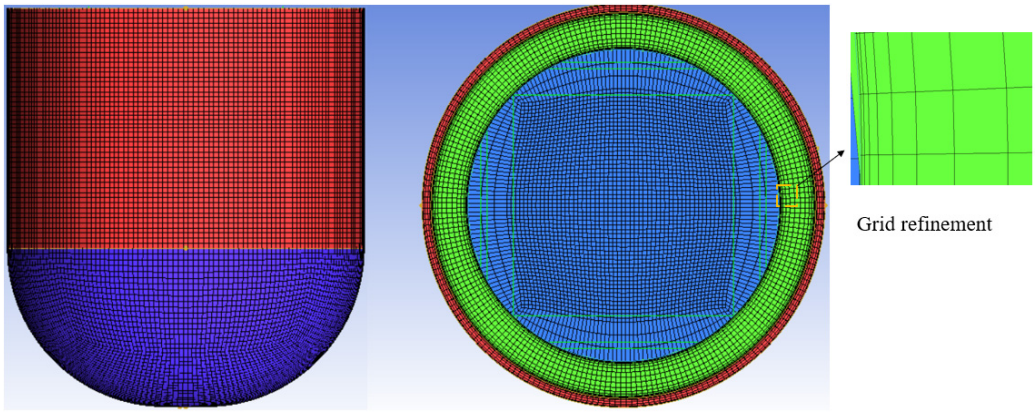


Figure 3. Mesh model of HML.

2.5. Boundary Conditions

The fluid dynamics software FLUENT 2023 R1 is used to calculate and solve the mesh model. The coupling model with solid and fluid volumes is applied in this paper. As fluids, HM and air interact with the surrounding solid material. However, the flow velocity of hot metal and air is small, which has less effect on the solid. Therefore, only the effect of solids on the fluid flow is considered. This is one-way coupling. The turbulent standard $k-\varepsilon$ model is used to solve the flow model for the simulation. The couple algorithm is applied to discretize all control equations. The residual convergence standard for the continuity equation, momentum equation and turbulence equation is 1×10^{-3}, while the convergence criterion for the energy equation is 1×10^{-6}. All control equations are discretely dispersed using a second-order welcoming style. The calculated domain boundary conditions are as follows:

(1) The heat exchange between the HML and the surrounding is shown in Equation (11), including convection and radiative heat transfer [24]:

$$Q_{loss} = h_0 \sum A_{w,i}(T_{w,i} - T_0) + \varepsilon\sigma \sum A_{w,i}\left(T_{w,i}^4 - T_0^4\right) \quad (11)$$

where σ is the Stefan–Boltzmann constant, 5.67×10^{-8} W/(m^2·K^4); $A_{w,i}$ is the area of the outer wall grid element i of the steel shell, m^2; $T_{w,i}$ is the temperature of the outer wall grid element i of the steel shell, K; T_0 is the ambient temperature, K; h_0 is the convective heat transfer coefficient, W/(m^2·K); ε is the emissivity of the wall material.

(2) The interface of slag iron is a free sliding wall. The internal layers of the HML are treated as heat transfer coupling boundaries.

The thermophysical parameters of different materials are shown in Table 1 [25,26]. The temperature of firebrick changes greatly. Hence, its thermophysical parameters change obviously, which may have a great effect on the heat transfer of HM. During the simulation, the temperature of other materials changed little. Therefore, these thermophysical parameters are treated as fixed values in order to improve the efficiency and stability of the numerical simulation. The temperature change and composition change of HM are very small. The physical properties, such as density, specific heat capacity, thermal conductivity and viscosity of HM, can be calculated using JMATPRO v9.0 software. The physical property parameters of HM are shown in Table 2. Referring to the on-site temperature measurement results, the initial conditions of the calculation domain are shown in Table 3.

According to the Chinese National Standard GB/T 28591-2012, "Wind scale", air velocity refers to the horizontal distance of air movement per unit time [27]. The air velocity, ambient temperature, slag thickness and furnace cover thickness parameters of the 30 cases (case A1–case F5) simulated are shown in Table 4. It is pointed out here that the air velocity and ambient temperature of the surroundings during HM transportation vary in different weather conditions. In the process of taking parameters, the values of air velocity and ambient temperature in normal weather are considered. Therefore, the

ambient temperature is gradually increased from −20 °C (A1) to a maximum level of 40 °C (A5). The air velocity is increased from 0 (C1) to 12 m/s (C5) when the ambient temperature is kept at 25 °C. Based on the wind scale, an air velocity of 12 m/s is within the sixth level range, also known as strong wind. It is sometimes present during HM transportation. Meanwhile, considering the slag removal operation, the value of slag thickness is from 0 to 250 mm (E5). When the HM is not covered by slag, the furnace cover with different thicknesses is added to the HML (case F1–case F5).

Table 1. Thermophysical parameters of different materials.

Material	Thermal Conductivity (W/(m·K))	Density (kg/m^3)	Specific Heat (J/(kg·K))	Emissivity
Steel shell	46.67	7600	502.8	0.85
Al_2O_3-SiC-C Firebrick	1.4×10^{-3} t + 0.3011	3200	0.198 t + 842.73	0.45
Slag	2.00	2600	1200.0	0.60
Air	0.085	0.257	1.197	0

Table 2. Physical property parameters of HM.

Thermal Conductivity (W·m^{-1}·K^{-1})	Density (kg/m^3)	Specific Heat (J/(kg·K))	Coefficient of Thermal Expansion (K^{-1})	Viscosity (Pa·s)	Emissivity
23.26	7100	879.00	0.0002	0.0065	0.6

Table 3. Initial conditions of domains.

Compute Domains	HM	Air	Slag	Firebrick	Steel Shell
Initial temperature (°C)	1321	1100	1321	1050	300

Table 4. Numerical schemes for distributing HM in HML.

Case	Ambient Temperature (°C)	Air Velocity (m/s)	Slag Thickness (mm)	Furnace Cover Thickness (mm)
A1	−20	0	0	0
A2	−5	0	0	0
A3	10	0	0	0
A4	25	0	0	0
A5	40	0	0	0
B1	−20	0	150	0
B2	−5	0	150	0
B3	10	0	150	0
B4	25	0	150	0
B5	40	0	150	0
C1	25	0	0	0
C2	25	3	0	0
C3	25	6	0	0
C4	25	9	0	0
C5	25	12	0	0
D1	25	0	150	0
D2	25	3	150	0
D3	25	6	150	0
D4	25	9	150	0
D5	25	12	150	0
E1	25	12	50	0

Table 4. *Cont.*

Case	Ambient Temperature (°C)	Air Velocity (m/s)	Slag Thickness (mm)	Furnace Cover Thickness (mm)
E2	25	12	100	0
E3	25	12	150	0
E4	25	12	200	0
E5	25	12	250	0
F1	25	12	0	50
F2	25	12	0	100
F3	25	12	0	150
F4	25	12	0	200
F5	25	12	0	250

2.6. Theoretical Calculations

Due to the large temperature difference of each part of the ladle, the natural convection heat transfer coefficients in the boundary conditions vary greatly. It is necessary to obtain accurate convective heat transfer coefficients. The classical theory in heat transfer is used to calculate the natural convection heat transfer coefficient as well as the forced convection heat transfer coefficient at different air velocities [26].

The convective heat transfer between air and the wall surface of the HML can be regarded as the natural convection of large space under uniform wall temperature boundary conditions. t_w is the wall temperature, and t_f is the ambient temperature. The following form of experimental correlation is widely used in engineering calculation:

$$Nu_m = C(GrPr)_m^n \tag{12}$$

where Nu_m is the Nu of the average surface heat transfer coefficient, and m represents the arithmetic mean temperature of the boundary layer. The qualitative temperature expression is $t_m = \left(t_w + t_f\right)/2$. C and n are determined by the Gr. In the case of natural convection in a large space of a transverse cylinder, the expression of the Gr is

$$Gr = \frac{g a_v \Delta t l^3}{v^2} \tag{13}$$

where the Δt in the Gr is the difference between t_w and t_f, K; the expansion coefficient expression for ideal gases is $a_v = 1/T$, K^{-1}; g is the acceleration of gravity, m/s^2; l is the characteristic length, m; v is the viscosity of air at the arithmetic mean temperature, m^2/s.

Through calculation, it is found that during the heat transfer process of HML, the Gr is greater than 4.65×10^9; therefore, C is set as 0.11, and n is set as 0.3333. Pr is set as 0.68 and 0.708 at 200 °C and 700 °C, respectively. The value is calculated to obtain the Nu_m. The relationship between the Nu_m and the natural convection heat transfer coefficient is as follows:

$$Nu_m = \frac{hl}{\lambda} \tag{14}$$

where h is the natural convection heat transfer coefficient, $W/(m^2 \cdot K)$; l is the characteristic length, m; and λ is the thermal conductivity of air, $W \cdot m^{-1} \cdot K^{-1}$. Therefore, the size of the natural convective heat transfer coefficient of each part of the HML can be calculated, as shown in Table 5.

Table 5. Natural convective heat transfer coefficient of each part.

Material	Steel Shell/Furnace Cover	Firebrick	Slag
h ($W/(m^2 \cdot K)$)	6.06	5.91	5.13

At different air velocities, the total convective heat transfer coefficient is the sum of the forced convection heat transfer coefficient and the natural convection heat transfer coefficient. Therefore, it is necessary to calculate the forced convection heat transfer coefficient separately and finally obtain the total convective heat transfer coefficient.

The forced convection heat transfer phenomenon of the HML can be approximated as a single tube of fluid sweeping the circular section. The average surface heat transfer coefficient of a fluid sweeping the round tube can be expressed by the following correlation:

$$Nu = CRe^n Pr^{\frac{1}{3}} \tag{15}$$

where Re and Pr are the characteristic numbers of air. The qualitative temperature is t_m; the characteristic length is the outer diameter of the tube; and the characteristic velocity is the channel flow velocity; C and n are determined by Re. For the steel shell, the Re is the Re of external air flowing through the steel shell at a certain velocity. It represents the ratio of the inertial force to the viscous force of the air flowing through the steel shell. The expression for Re is as follows:

$$Re = \frac{ul}{v} \tag{16}$$

where u is the air flow rate, m/s; l is the diameter of the steel shell, m; v is the viscosity of the air at a qualitative temperature, m^2/s. When the air passes through the slag and firebrick, the Re is obtained in the same way. Through calculation, the calculated values of Re are obtained, as shown in Table 6.

Table 6. Calculated values of Re in HML at different air velocities.

Air Velocity	Re of Steel Shell	Re of Firebrick	Re of Slag
3 m/s	174,418	66,137	35,095
6 m/s	348,837	132,275	70,190
9 m/s	523,255	198,412	105,286
12 m/s	697,674	264,550	140,381

In Table 6, the calculated values of Re are greater than 40,000; therefore, C and n are set as 0.0266 and 0.805, respectively. Equation (15) is calculated to obtain the forced convection heat transfer coefficient at different air velocities. Finally, it is added with the natural convective heat transfer coefficient to obtain the total convective heat transfer coefficient, as shown in Table 7 below.

Table 7. Calculated h_f values of HML at different air velocities.

Air Velocity	h_f of Steel Shell ($W/(m^2 \cdot K)$)	h_f of Firebrick ($W/(m^2 \cdot K)$)	h_f of Slag ($W/(m^2 \cdot K)$)
3 m/s	14.77	11.8	10.43
6 m/s	21.27	16.21	14.51
9 m/s	27.14	20.19	18.13
12 m/s	32.64	23.91	21.31

3. Model Validation

To obtain numerical results at low computational cost and with high accuracy, mesh independence verification of case E2 is carried out. Three different mesh densities of 0.3 million, 0.5 million and 1.5 million are generated for the same model. The HM end temperature of three different mesh densities is obtained, as shown in Table 8. It could be concluded that the mesh with 0.5 million grids can satisfy the result accuracy and reduce the calculation time.

Table 8. The mesh independent assessment.

Grid Number	Charging Temperature (°C)
0.3 million	1307.563
0.5 million	1309.011
1.5 million	1309.474

Meanwhile, the on-site measurement was applied to ensure the correctness of the simulation results. Figure 4 depicts the insertion of a high-temperature thermocouple into the HM. Based on some preliminary simulation work, it was found that the temperature approximately 0.3 m below the surface of the HM can be considered as the average temperature of the HM. By measuring the temperature of HM from multiple HMLs, the average value is set as the result of on-site temperature measurement. Through the actual measurement of the site, the ambient temperature is 26 °C; the wind level is 4; and the weather is cloudy. The thickness of the slag in the ladle is about 106 mm, and there is no furnace cover. These are roughly the same simulation parameters as in case E2. Therefore, the temperature measurement data can be used to verify the simulation results of case E2. The numerical results under the same condition were compared with the average field measurement of HM temperature, as shown in Table 9. The temperature difference between the numerical result and experimental result was 1 °C. The relative error of temperature drop was 0.07%, which met the requirements of model verification. It could be concluded that the mathematical method model of HML heat transfer simulation was applicable to this work.



Figure 4. On-site temperature measurement.

Table 9. Comparison of measurement results and simulation results.

Time	Measured Temperature	Simulated Temperature	Error	Relative Error
50 min	1308 °C	1309 °C	1 °C	0.07%

4. Results and Discussion

4.1. Effect of Ambient Temperature on Temperature Drop of HM

Ambient temperature is a parameter that may affect the temperature drop of HM. This section discusses the influence of ambient temperature on the temperature drop of HM without slag coverage and HM with a slag thickness of 150 mm.

Figure 5 shows the temperature drop of HM without slag coverage by varying the ambient temperature from −20 °C to 40 °C, where the transportation time is 50 min, and air

velocity is 0 m/s. The temperature drop of the HM only changed slightly. The temperature drop curve is almost a horizontal line. When the ambient temperature is −20 °C, the temperature drop of HM is 55.29 °C. When the ambient temperature increases to 40 °C, the temperature drop of HM is 55.17 °C. The temperature drop difference is only 0.12 °C. For the HM without slag coverage, the change in ambient temperature has little effect on the temperature drop of HM. Therefore, even if the slag is completely removed in the future, it is not necessary to consider the influence of ambient temperature on the temperature drop of HM.

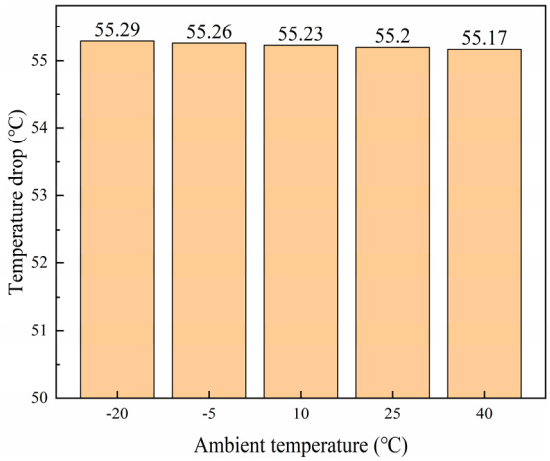


Figure 5. The temperature drop of HM without slag coverage by varying the ambient temperature from −20 °C to 40 °C.

As shown in Figure 6, the temperature distributions of the HM in scheme A exhibit minimal differences. The HM has no thermal stratification at any ambient temperature. The temperature gradient of the HM is very small, except for the region close to the air. The maximum temperature and minimum temperature of HM are almost unchanged with the increase in ambient temperature. Through thermal resistance analysis, it is found that the upper part of the HM without slag coverage undergoes direct heat exchange with the air, resulting in strong convective and radiative heat transfer and low thermal resistance. However, heat dissipation from the HM in other directions encounters thermal resistance introduced by the HML, leading to higher thermal resistance due to its lower thermal conductivity. Therefore, the temperature of the upper layer is the lowest, and the overall heat dissipation of the HM remains substantial. Due to changes in ambient temperature, the temperature difference between the HM and the environment also varies. However, since the temperature difference between the HM and the environment is approximately 1300 °C, even with only slight fluctuations in ambient temperature, the change in temperature difference is not significant. Additionally, the significant thermal resistance introduced by the HML further diminishes the impact of changes in ambient temperature.

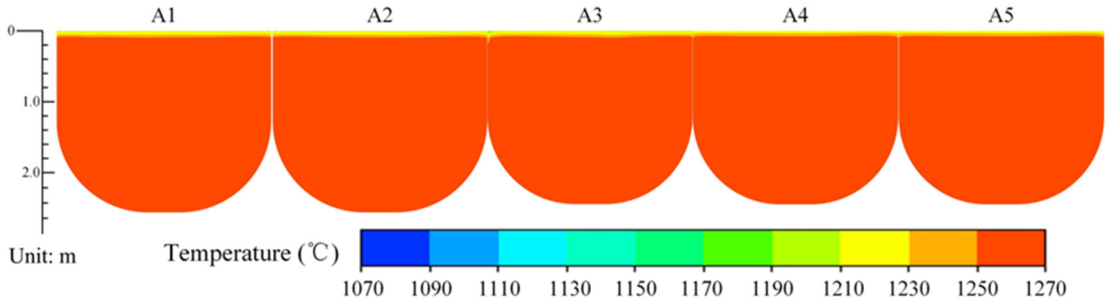


Figure 6. Temperature distributions of the longitudinal section of HM in scheme A.

In order to reduce heat loss from the HM, the steel plants do not carry out slag removal during HM transportation. Figure 7 shows the effect of ambient temperature on the temperature drop of HM with a slag thickness of 150 mm by varying the ambient temperature from −20 °C to 40 °C. Note that the temperature drop is 10.33 °C when the ambient temperature is 40 °C, while it increases to 10.37 °C when the ambient temperature is reduced to −20 °C. The temperature drop difference is only 0.04 °C. This implies that lowering the ambient temperature could not noticeably influence the temperature drop of HM with a slag thickness of 150 mm. Hence, it is unnecessary to consider the influence of ambient temperature on the temperature drop of HM for steel plants. A comparison with Figure 5 indicates that the temperature drop of HM with a slag thickness of 150 mm is 45 °C lower than that of HM without slag coverage. The slag layer could exert a good heat preservation effect on HM. With the decrease in ambient temperature, the heat preservation effect is more obvious.

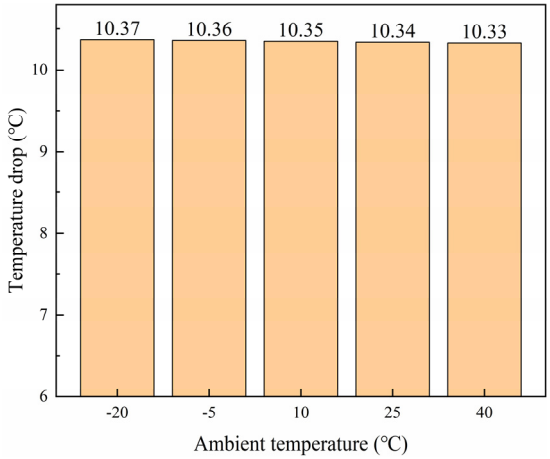


Figure 7. Temperature drop of HM with slag thickness of 100 mm by varying the ambient temperature from −10 °C to 50 °C.

Figure 8 shows the temperature distributions of the longitudinal section of HM and slag in scheme B. In scheme B, each case exhibits nearly identical temperature distributions. Due to the protection provided by the slag, the influence of changes in ambient temperature is further reduced, to the extent that the temperature drop between adjacent cases differs by only 0.01 °C. The temperature of HM is obviously higher compared with the HM without slag coverage. The slag substitutes for HM in the comprehensive heat transfer of convection and radiation with the environment. This initially results in the maintenance of the HM temperature at 1310 °C. The thermal resistance in other directions is also relatively low. Thus, the overall temperature of HM decreases slowly.

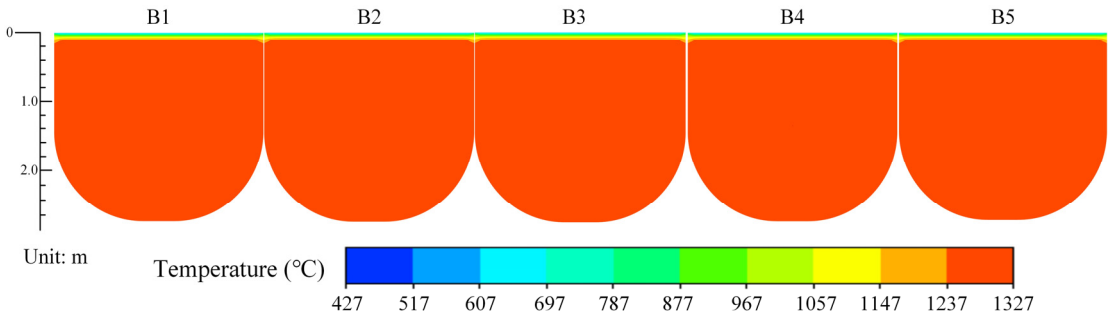


Figure 8. Temperature distributions of the longitudinal section of HM and slag in scheme B.

4.2. Effect of Air Velocity on Temperature Drop of HM

Air velocity may affect the temperature drop of HM. This section discusses the influence of ambient temperature on the temperature drop of HM without slag coverage and HM with a slag thickness of 150 mm. As depicted in Figure 9, the temperature drop of HM has a significant upward trend with the increase in air velocity. Its linear degree is high. When the air velocity is 0 m/s, the temperature drop is 55.21 °C, while when the air velocity is 12 m/s, the temperature drop is 59.71 °C. The temperature drop difference is 4.5 °C. The change in air velocity had a great influence on the temperature drop of HM. Therefore, it was necessary to consider the effect of air velocity for the HM without slag coverage.

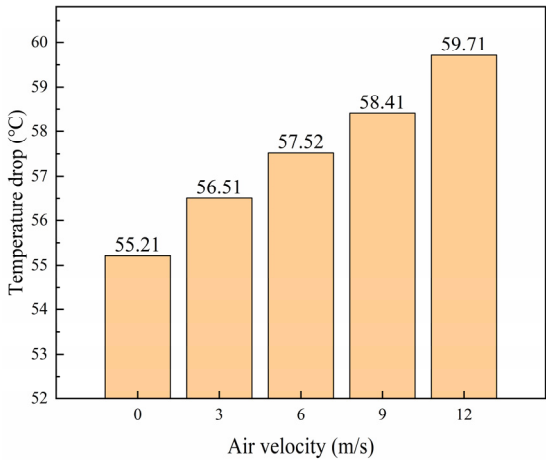


Figure 9. Temperature drop of HM without slag coverage by varying the air velocity from 0 m/s to 12 m/s.

Figure 10 shows the temperature distributions of the longitudinal section of HM in scheme C. It is observed that the high-temperature zone of the HM decreases with an increase in air velocity. With an increase in air velocity, the convective heat transfer coefficient notably increases, resulting in a decrease in convective heat transfer resistance on the air side and consequently leading to increased convective heat transfer of the HM. However, since radiative heat transfer predominates for the high-temperature object, the lowest temperature of the HM in case C5 is approximately 20 °C lower than that in case C1. The good thermal conductivity and certain fluidity of HM result in very low internal thermal resistance within the HM. Therefore, the low temperature of the upper layer of HM can quickly spread throughout the HM, leading to increased heat loss from the molten iron in case C5.

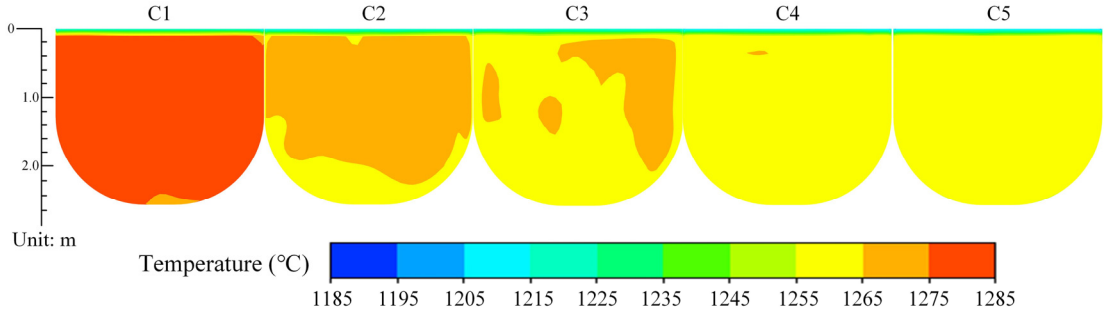


Figure 10. Temperature distributions of the longitudinal section of HM in scheme C.

As shown in Figure 11, the temperature drop of HM increases with the increase in air velocity. However, the trend is not obvious. When the air velocity is 0 m/s, the temperature drop is 10.34 °C, while when the air velocity is raised to 12 m/s, the temperature drop is 10.38 °C. The temperature drop difference is only 0.01 °C. On high-temperature occasions,

the radiation heat transfer is dominant. The increase in air velocity only improves the convective heat transfer coefficient of convective heat transfer. Even if the air velocity increases, the slag still exerts a good heat preservation effect. Therefore, the influence of air velocity on the average temperature of HM is generally not considered.

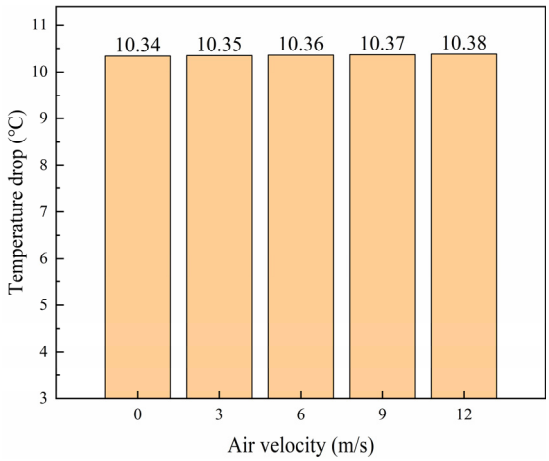


Figure 11. Temperature drop of HM with slag thickness of 100 mm by varying the air velocity from 0 m/s to 12 m/s.

Figure 12 represents the temperature distributions of the longitudinal section of HM and slag in scheme D. The temperature distributions of HM hardly are almost unchanged by air velocity, which explains that the temperature drop of HM increases only slightly with the increase in air velocity. When the air velocity increases, the convective heat transfer capacity between the HML and the environment is enhanced. The high thermal resistance of the ladle and the significant thermal resistance determined by the low thermal conductivity of the slag together protect the HM, reducing the influence of external heat exchange.

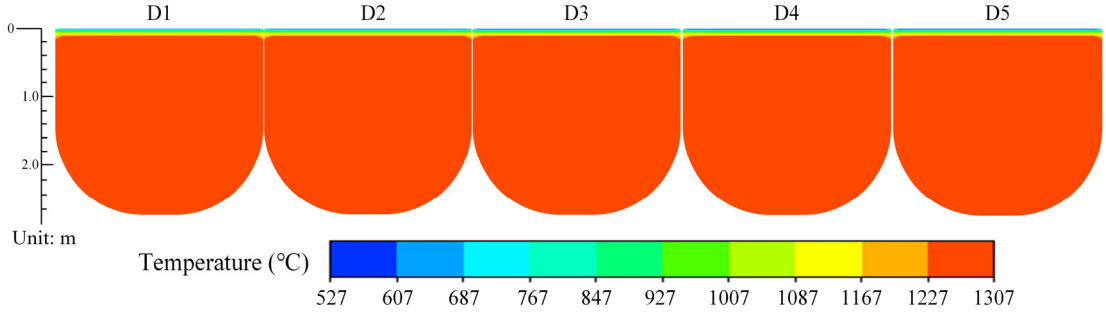


Figure 12. Temperature distributions of the longitudinal section of HM and slag in scheme D.

4.3. Effect of Slag Thickness on Temperature Drop of HM

As described in the previous two sections, the slag can well reduce the influence of ambient temperature and air velocity and exert a significant insulation effect. However, the slag brings impurities to the EAF steelmaking process, which increases the load of impurity removal and energy consumption. Therefore, it is necessary to study the appropriate slag thickness for insulation.

As depicted in Figure 13, the temperature drop of HM has a significant downward trend with the increase in slag thickness. However, when the slag thickness reaches 150 mm, the further improvement in heat retention by increasing the slag thickness becomes little. When the slag thickness is 150 mm, the temperature drop of HM is 10.38 °C, while when the slag thickness is raised to 250 mm, the temperature drop of HM is 10.26 °C. The difference between the 150 mm and 250 mm slag thickness is negligible. The minor increase of 4.68 °C

is noticed in the temperature drop of HM for the 50 mm slag layer thickness compared to the 150 mm slag layer.

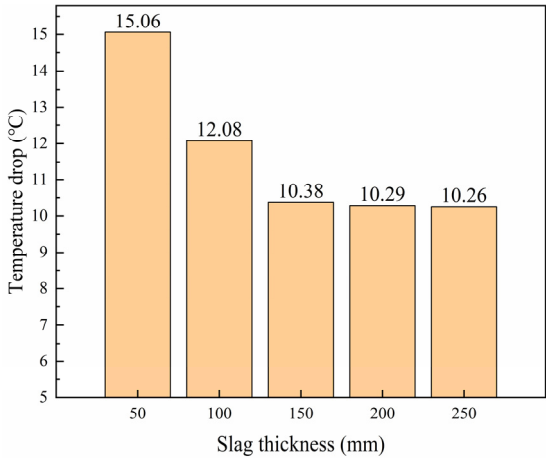


Figure 13. Temperature drop of HM with different slag thicknesses.

Figure 14 shows the temperature distributions of the longitudinal section of HM in scheme E. It is found that the thicker the slag layer, the larger the area of the high-temperature zone of the HM. In case E1, due to only 50 mm slag thickness, the thermal resistance above is smaller compared to other directions, resulting in a lower temperature of the HM above. When the slag thickness is 150 mm, the thermal resistance above is greater than in other directions, resulting in the temperature of the molten iron above remaining at 1311 °C. As the heat exchange above is already minimal, there is no need to increase the slag thickness to compensate for this deficiency.

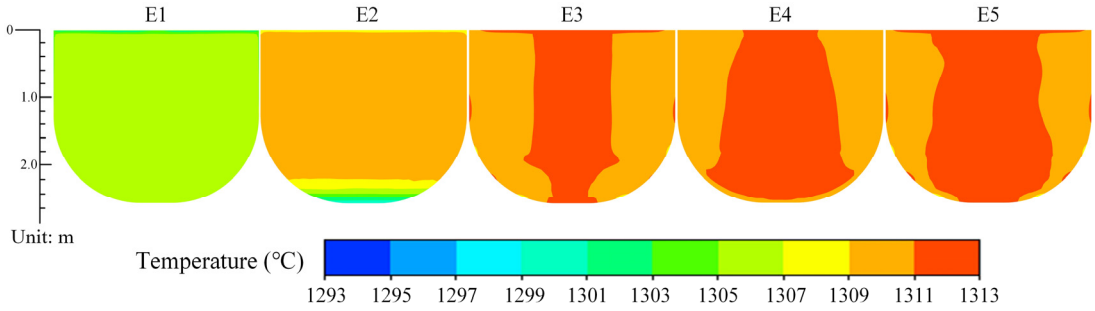


Figure 14. Temperature distributions of the longitudinal section of HM in scheme E.

4.4. Effect of Furnace Cover Thickness on Temperature Drop of HM

As slag is burdensome for the EAF steelmaking process, the furnace cover is considered as a replacement for slag to insulate the HM. Figure 15 represents the temperature drop of HM with different furnace cover thicknesses. When the furnace cover thickness is 50 mm, the temperature drop of the HM is 16.78 °C. It is evident that the furnace cover also has the ability to substantially reduce the temperature drop of the HM. The insulating effect of the furnace cover stems from the low thermal conductivity of refractory bricks and the presence of air. However, due to the increased convective heat transfer caused by air movement, the thermal insulation effect of a furnace cover is not as effective as that of slag with the same thickness. The minor increase of 0.61 °C is noticed in the temperature drop of HM for the 200 mm furnace cover thickness compared to the 200 mm slag layer. This is because an increase in furnace cover thickness not only increases the thermal resistance to conduction but also decreases the convective heat transfer resistance. There exists an optimal thickness in this regard, known as the critical insulation thickness or critical insulation diameter.

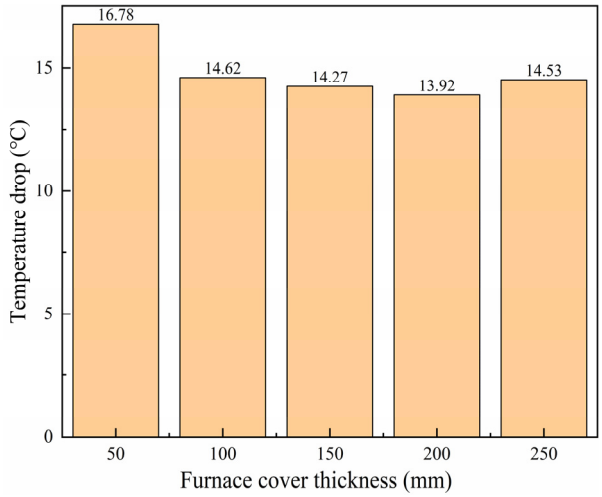


Figure 15. Temperature drop of HM with different furnace cover thicknesses.

As depicted in Figure 16, the area of the high-temperature zone in the HM first increases and then decreases with the increase in furnace cover thickness. However, the temperature above the HM is relatively low, indicating that the thermal resistance of the air is still greater than that in other directions. Adding a small amount of slag can increase the thermal resistance on the air side, which can make the insulation effect more pronounced. In case F5, when the furnace cover thickness is excessive, this initially results in dissipation of internal air heat, leading to an overall decrease in air temperature within the range of 2–5 °C. This temperature drop indirectly causes a lower temperature above the HM. This is somewhat contrary to everyday experience.

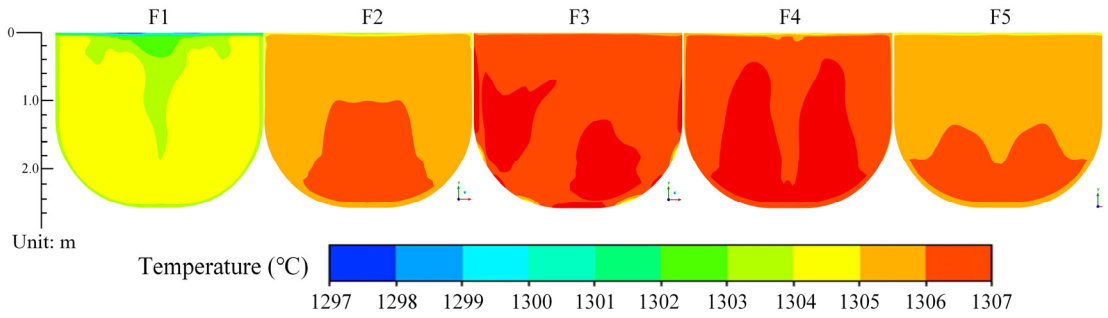


Figure 16. Temperature distributions of the longitudinal section of HM in scheme F.

4.5. Multiple Linear Regression for Temperature Drop of HM

To facilitate the database to directly calculate the temperature of HM into the furnace, it is necessary to quantify the temperature drop during the transportation of HM. Considering the interdependencies of the different effects when setting up the equation, the situations are divided into two categories, respectively: with slag and without slag. At the same time, ridge regression is applied to deal with collinearity of independent variables. Based on the numerical simulation results of the previous four sections, two multivariate linear function expressions of temperature drop in different situations are obtained. When the HM is not covered by slag, only the ambient temperature, air velocity and time affect the temperature drop of HM. The multivariate linear function expression is shown in Equation (17). Based on the significance of the F-test, the *p*-value is within 1%, indicating that there is a regression relationship between the independent variable and the dependent variable. The goodness of fit R^2 of the expression is 0.989, which fits the numerical simulation results.

$$\Delta t = (55.32 - 0.001x_1 + 0.335x_2)T/50 \quad (17)$$

where Δt is the temperature drop of HM, °C; x_1 is the ambient temperature, °C; x_2 is the air velocity, m/s; T is the transportation time of HM, minute.

When the HM is covered by slag, only the slag thickness, furnace cover thickness and time affect the temperature drop of HM. The multivariate linear function expression is presented in Equation (18). The goodness of fit R^2 of the expression is 0.813, which also fits the numerical simulation results.

$$\Delta t = (14.92 - 0.02x_3 - 0.002x_4)T/50 \quad (18)$$

where Δt is the temperature drop of HM, °C; x_3 is the ambient temperature, °C; x_4 is the air velocity, m/s; T is the transportation time of HM, minute.

5. Conclusions

In this paper, the heat transfer behavior of HM during transportation is simulated by numerical simulation. The influence of ambient temperature, air velocity, slag thickness and furnace cover thickness on the temperature drop of HM is studied. The conclusions are as follows:

(1) The change in ambient temperature and air velocity has no obvious effect on the temperature drop of HM with a slag thickness of 150 mm. The influence of the above two factors on the temperature drop of HM is not considered when the HM is covered with slag in steel plants.

(2) The ambient temperature has little effect on the temperature drop of HM without slag coverage. Even for the HM without slag coverage, it is not necessary to consider the influence of ambient temperature on the temperature drop of HM.

(3) Air velocity has a great influence on the temperature drop of HM without slag coverage. When the air velocity is 0 m/s, 3 m/s, 6 m/s, 9 m/s and 12 m/s, the temperature drop of HM is 55.21 °C, 56.51 °C, 57.52 °C, 58.41 °C and 59.71 °C, respectively.

(4) If there is no furnace cover, a certain amount of slag is required for insulation. When the slag thickness is 150 mm, it is most suitable. This effectively increases the thermal resistance above the HM to a sufficient extent.

(5) The furnace cover can effectively substitute for slag in providing insulation for the HM. However, in the absence of slag, it is not advisable to increase the thickness of the furnace cover excessively. During this heat dissipation process, there exists a critical insulation thickness.

(6) Through multiple linear regression analysis, the function expression of HM temperature drop is $\Delta t = (55.32 + 0.001x_1 + 0.335x_2)T/50$ and $\Delta t = (14.92 - 0.02x_3 - 0.002x_4)T/50$. This can accurately predict the temperature drop of HM and determine the energy of HM before entering the EAF.

This study can help develop targeted insulation measures and determine the temperature of HM. Therefore, the variable energy of HM entering the furnace is accurately obtained rather than a constant given by experience, which is expected to control the input energy for deep energy-saving optimization in the EAF steelmaking process [28]. However, when the shape and capacity of the ladle change, the temperature drop of the HM will also change. In order to obtain a polynomial suitable for other shapes and capacities of ladles, it is only necessary to change the geometric model of the ladle. A numerical method for predicting HM temperature drop is provided.

Author Contributions: W.C.: Methodology, Software, Validation, Investigation, Data Curation, Writing—Original Draft, Visualization, Funding Acquisition; H.H.: Methodology, Formal Analysis, Resources, Writing—Review and Editing, Funding Acquisition, Project Administration; S.W.: Software, Validation, Data Curation; F.C.: Visualization, Formal Analysis, Data Curation; Y.G.: Resources, Conceptualization, Supervision; L.Y.: Conceptualization, Methodology, Software, Resources, Writing—Review and Editing, Supervision. All authors have read and agreed to the published version of the manuscript.

Funding: This research was supported by the National Natural Science Foundation of China (No. 52174328) and the Fundamental Research Funds for the Central Universities of Central South University (No. 2023XQLH027 and No. 2024ZZTS0062).

Data Availability Statement: The raw data supporting the conclusions of this article will be made available by the authors on request.

Conflicts of Interest: The authors declare no conflicts of interest.

References

1. Echterhof, T. Review on the Use of Alternative Carbon Sources in EAF Steelmaking. *Metals* **2021**, *11*, 222. [CrossRef]
2. Dock, J.; Kienberger, T. Techno-economic case study on Oxyfuel technology implementation in EAF steel mills—Concepts for waste heat recovery and carbon dioxide utilization. *Clean. Eng. Technol.* **2022**, *9*, 100525. [CrossRef]
3. Yang, Z.; Yang, L.; Cheng, T.; Chen, F.; Zheng, F.; Wang, S.; Guo, Y. Fluid flow characteristic of EAF molten steel with different bottom-blowing gas flow rate distributions. *ISIJ Int.* **2020**, *60*, 1957–1967. [CrossRef]
4. Ekmekçi, I.; Yetisken, Y.; Çamdali, U. Mass balance modeling for electric arc furnace and ladle furnace system in steelmaking facility in Turkey. *J. Iron Steel Res. Int.* **2007**, *14*, 1–6. [CrossRef]
5. Jie, F.U.; Zhong-Binge, W.A.N.G.; Xing-Jiang, W.A.N.G.; Xin-Ping, M. Advances in modern EAF steelmaking technology of China. *J. Iron Steel Res. Int.* **2004**, *11*, 1–9.
6. Tomažič, S.; Andonovski, G.; Škrjanc, I.; Logar, V. Data-Driven Modelling and Optimization of Energy Consumption in EAF. *Metals* **2022**, *12*, 816. [CrossRef]
7. Omotani, M.A.; Heaslip, L.J.; Mclean, A. Ladle temperature control during continuous casting. *Iron Steelmak.* **1983**, *10*, 29–35.
8. Zeng, X.N. Theoretical analysis of reducing temperature drop of HM in transportation. *Metall. Energy* **1996**, *15*, 27–31.
9. Pan, Y.; Björkman, B. Physical and mathematical modelling of thermal stratification phenomena in steel ladles. *ISIJ Int.* **2002**, *42*, 614–623. [CrossRef]
10. Du, T.; Cai, J.J.; Li, Y.J.; Wang, J.J. Analysis of Hot Metal Temperature Drop and Energy-Saving Mode on Techno-Interface of BF-BOF Route. *Iron Steel* **2008**, *43*, 83–86+91. [CrossRef]
11. Zimmer, A.; Lima, N.C.; Trommer, R.M.; Bragança, S.R.; Bergmann, C.P. Heat transfer in steelmaking ladle. *J. Iron Steel Res. Int.* **2008**, *15*, 11–14. [CrossRef]
12. Tripathi, A.; Saha, J.K.; Singh, J.B.; Ajmani, S.K. Numerical simulation of heat transfer phenomenon in steel making ladle. *ISIJ Int.* **2012**, *52*, 1591–1600. [CrossRef]
13. Putan, V.; Vilceanu, L.; Socalici, A.; Putan, A. Mathematical and physical modeling of thermal stratification phenomena in steel ladles. *IOP Conf. Ser. Mater. Sci. Eng.* **2018**, *294*, 012004. [CrossRef]
14. Glaser, B.; Görnerup, M.; Sichen, D. Thermal modelling of the ladle preheating process. *Steel Res. Int.* **2011**, *82*, 1425–1434. [CrossRef]
15. Deodhar, A.; Singh, U.; Shukla, R.; Gautham, B.P.; Singh, A.K. Fast and accurate prediction of stratified steel temperature during holding period of ladle. *Met. Mater. Trans. B* **2016**, *48*, 1217–1229. [CrossRef]
16. Yang, G.; Xu, A.J.; He, D.F. Review on temperature drop of HM from BF to BOF. *China Metall.* **2018**, *28*, 1–6. [CrossRef]
17. Díaz, J.; Fernández, F.J.; Prieto, M.M. Hot Metal Temperature Forecasting at Steel Plant Using Multivariate Adaptive Regression Splines. *Metals* **2019**, *10*, 41. [CrossRef]
18. Zhang, H.; Zhou, P.; Yuan, F. Effects of ladle lid or online preheating on heat preservation of ladle linings and temperature drop of molten steel. *Energy* **2020**, *214*, 118896. [CrossRef]
19. Cheng, T.; Zhu, R.; Dong, K. Effect of methane-hydrogen mixtures on flow and combustion of coherent jets. *J. Iron Steel Res. Int.* **2017**, *24*, 1143–1151. [CrossRef]
20. He, Y.-B.; Guo, W.-K.; Li, Y.-H.; Liu, G.-M.; Cui, X. Numerical simulation of flow characteristics of side-bottom combined blowing in iron bath reactor. *J. Iron Steel Res. Int.* **2023**, *30*, 236–248. [CrossRef]
21. Liu, F.; Sun, D.; Zhu, R.; Fan, S. Behaviors of coherent flow field with various shrouding nozzles arrangement. *ISIJ Int.* **2018**, *58*, 496–504. [CrossRef]
22. Yan, H.; Conejo, A.N.; Zhang, H.; Feng, W.H.; Niu, K.J. Numerical simulation of heat transfer during ladle holding period. *Contin. Cast.* **2022**, *1*, 31–38. [CrossRef]
23. Zuo, W.E.J.; Lin, R.; Jin, Y.; Han, D. Numerical investigations on different configurations of a four-channel meso-scale planar combustor fueled by hydrogen/air mixture. *Energy Convers. Manag.* **2018**, *160*, 1–13. [CrossRef]
24. Li, H.X. *Manual of Refractory Material*; Metallurgical Industry Press: Beijing, China, 2010.
25. Visloguzova, A.; Kashcheev, I.D.; Serova, L.V.; Khoroshikh, M.A. Corundum-periclase-carbon refractories for lining steel-pouring ladles. *Refract. Ind. Ceram.* **2010**, *51*, 9–11. [CrossRef]
26. Yang, S.M.; Tao, W.S. *Heat Transfer*; Higher Education Press: Beijing, China, 2006.

27. *GB/T 28591-2012*; Wind Scale. China Meteorological Administration: Beijing, China, 2012. Available online: https://www.nssi.org.cn/nssi/front/78168356.html (accessed on 3 March 2023).
28. Yang, L.; Li, Z.; Hu, H.; Zou, Y.; Feng, Z.; Chen, W.; Chen, F.; Wang, S.; Guo, Y. Evaluation of Energy Utilization Efficiency and Optimal Energy Matching Model of EAF Steelmaking Based on Association Rule Mining. *Metals* **2024**, *14*, 458. [CrossRef]

Disclaimer/Publisher's Note: The statements, opinions and data contained in all publications are solely those of the individual author(s) and contributor(s) and not of MDPI and/or the editor(s). MDPI and/or the editor(s) disclaim responsibility for any injury to people or property resulting from any ideas, methods, instructions or products referred to in the content.